Size Distributions Obtained from the Inversion of $I(Q)$ Using Integrated Light Scattering Spectroscopy

K. B. Strawbridge and F. R. Hallett*

Guelph–Waterloo Program for Graduate Work in Physics, Department of Physics, University of Guelph, Guelph, Ontario, Canada N1G 2W1

*Received August 24, 1993; Revised Manuscript Received January 25, 1994**

ABSTRACT: Traditionally, particle size distributions have been successfully obtained from dynamic light scattering (DLS) data. However, integrated light scattering (ILS) data in the form of $I(Q)$ vs Q contains more information about the particle, especially in the case of hollow or coated spheres where there are sensitivities to the refractive indices and coat thickness. The ILS technique is significantly faster in terms of both data collection and analysis, and number distributions are the immediate product of the inversion of $I(Q)$ vs Q data. Size distributions for both solid and hollow spheres have been obtained using a discrete inversion technique and nonnegative least squares which incorporate either Rayleigh–Gans–Debye (RGD) or Mie theories. The results are compared with size distributions obtained using DLS. In all cases examined, the ILS method proved to be more robust, requiring shorter data collection times and less stringent dependence on sample quality.

Introduction

Particle size information and, in particular, size distributions have always been of interest for a variety of systems such as polymers, microemulsions, and vesicles.[1-10] Although dynamic light scattering (DLS) spectroscopy has successfully yielded size distribution information on particles typically between 0.01 and 2 μm, another form of light scattering known as integrated light scattering (ILS) spectroscopy will be investigated as an alternate and complementary sizing technique.

A review of the literature revealed recent attempts to recover particle size distributions from ILS data. In our laboratory[11] it was determined that better agreement with ILS data could be obtained if polydispersity information was included in the analysis. Sheu[12] fit different types of assumed distribution functions to the ILS data. Finsy et al.[13] performed the inversion of simulated and experimental data using both the maximum entropy and a constrained regularization method, via Contin, on unimodal, bimodal, and trimodal distributions. However, in some instances, this produced abnormally narrow and sometimes spurious distributions. Also Schnablegger and Glatter[14] fit the inverse scattering data to a series of bell-shaped functions but did not assume any particular analytical form of the distribution. They simultaneously determined the size distribution and refractive index of colloidal particles. They also indicated that certain dominant particle parameters can be determined more precisely than others, and so they define a quality parameter to measure this sensitivity. All of these encouraging results led to the motivation to create a fitting program, based on discrete sampling methods, which would generate particle size distributions from the $I(Q)$ vs Q data. This method, which follows, has its origins in the exponential sampling technique initially described by Pike et al.[15] and later improved by Morrison et al.[16] A nonnegative least squares (NNLS) fit is applied using a predetermined range of radii and the RGD and Mie equations described below. The ILS technique is significantly faster than DLS in terms of both data collection and analysis times and yields number distributions directly. In the final analysis, the best understanding of any scattering system comes from data obtained from both experiments run concurrently. This is especially true when interparticle interactions could be significant.

Theory

Wyatt, using the Rayleigh–Gans–Debye (RGD) approximation,[17-22] determined a theoretical scattering intensity, $I(Q)_{TH}$, for a coated sphere with vertically polarized incident light to be[23]

$$I(Q)_{TH} = \left[\frac{m_2 - 1}{2\pi}\frac{4\pi r_2^3}{3}\left[\frac{3J_1(x)}{x} + f^3\frac{m_1 - m_2}{m_2 - 1}\frac{3J_1(fx)}{fx}\right]\right]^2 \quad (1)$$

where

$$m_1 = n_1/n_0, \quad m_2 = n_2/n_0, \quad f = 1 - t/r_2$$

t is the thickness of the coat and $J_1(x)$ is the first-order Bessel function with $x = Qr_2$. The variables n_0, n_1, and n_2 are the refractive indices of the medium, lumen, and coat, and r_1 and r_2 are the inner and outer radii, respectively. It is clear for the limiting case where the relative refractive indices m_1 and m_2 are equal that $I(Q)$ reduces to the expression obtained for that of a solid sphere. The magnitude of the scattering vector, Q, is defined as

$$Q = \frac{4\pi n_0}{\lambda_0}\sin\frac{\theta}{2} \quad (2)$$

where n_0 is the solvent refractive index, λ_0 is the wavelength of the light in vacuo, and θ is the scattering angle.

On the other hand, the scattered intensity from a coated-sphere system using Mie theory for vertically polarized incident light is given by[24,25]

$$I(Q)_{TH} = \frac{I_0}{kr^2}|S_1|^2 \quad (3)$$

where k is the wavenumber, r is the distance between the

* Abstract published in *Advance ACS Abstracts*, March 1, 1994.

0024-9297/94/2227-2283$04.50/0 © 1994 American Chemical Society

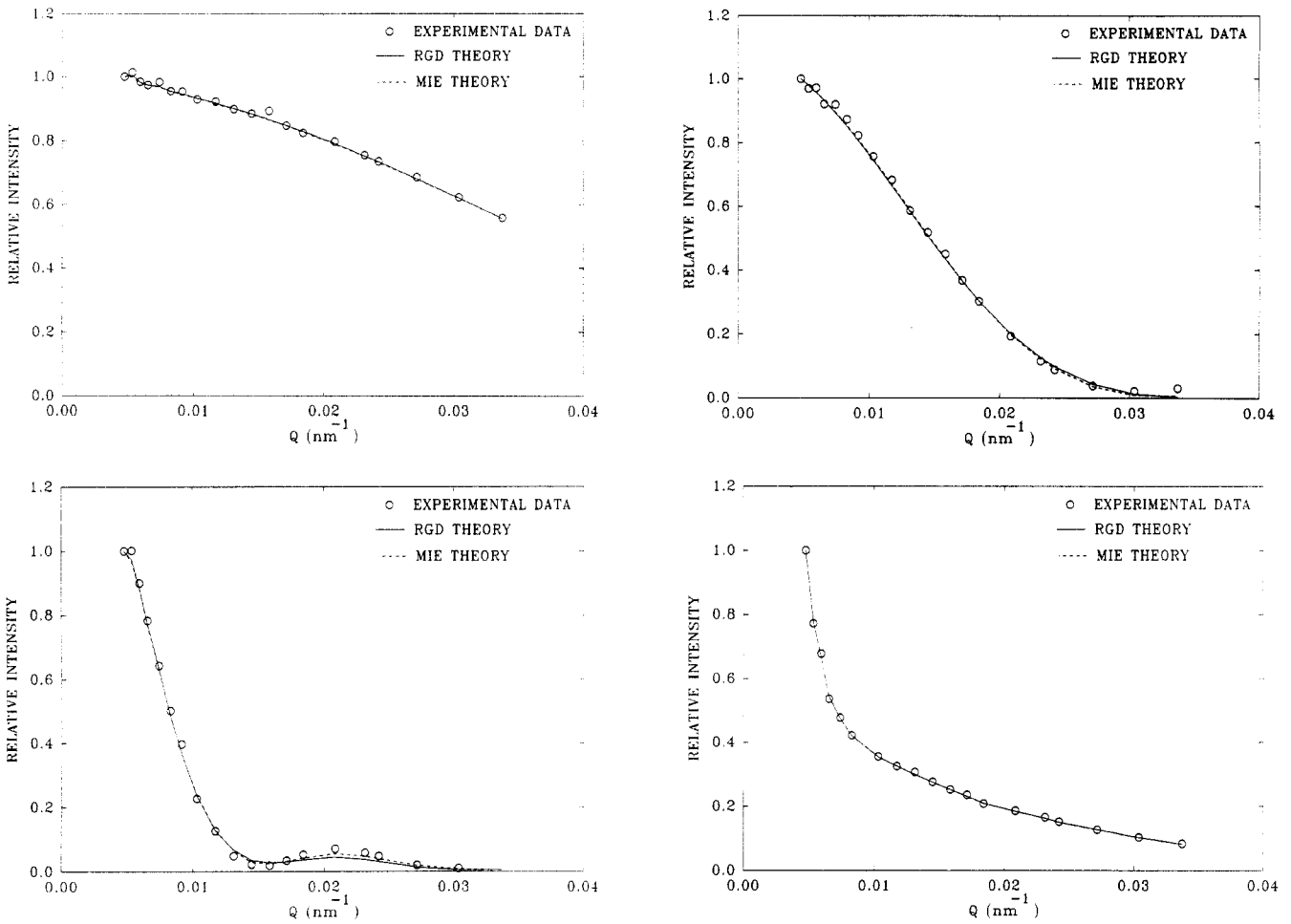

Figure 1. Plots of the relative intensity vs Q for (A, top left) 0.096-μm solid latex spheres, (B, top right) 0.269-μm solid latex spheres, (C, bottom left) hollow latex spheres, and (D, bottom right) DPPC/cholesterol vesicles showing a comparison between the fit obtained by using the RGD approximation and the Mie theory.

Table 1. Comparison of the Mean and Standard Deviations of the Distributions Obtained by ILS (Using both RGD and Mie Theories) and DLS[a]

	RGD		Mie		DLS	
sample	r_2 (μm)	std dev (μm)	r_2 (μm)	std dev (μm)	r_2 (μm)	std dev (μm)
0.096-μm-diameter latex spheres	0.044	0.0063	0.041	0.0085	0.040	0.0056
0.269-μm-diameter latex spheres	0.129	0.0077	0.122	0.0070	0.135	0.024
hollow latex spheres	0.244	0.022	0.227	0.020	0.192	0.047
DPPC/cholesterol vesicles	0.056	0.045	0.054	0.048	0.053	0.017

[a] Note that the standard deviation is a characteristic of the width of the distribution and not an uncertainty in the mean.

scattering particle and the point of the intensity measurement, and

$$S_1(\cos\theta) = \sum_{n=1}^{\infty} \frac{2n+1}{n(n+1)}(a_n\pi_n + b_n\tau_n) \qquad (4)$$

The angle-dependent functions are

$$\pi_n = \frac{P_n^1(\cos\theta)}{\sin\theta} \quad \text{and} \quad \tau_n = \frac{dP_n^1(\cos\theta)}{d\theta}$$

where $P_n^1(\cos\theta)$ is the associated Legendre polynomial and the scattering coefficients a_n and b_n for a coated sphere are given elsewhere.[25]

To obtain the size distribution, $G(r)$, the following equation must be solved:

$$I(Q) = \int_0^\infty I(Q,r)_{TH}\, G(r)\, dr \qquad (5)$$

However, the inversion is ill-conditioned, a problem well documented in the inversion of DLS data. An estimate can be obtained by using a discrete method involving a range and spacing of predetermined trial radii. The trial radii, between r_{min} and r_{max}, can be distributed either geometrically or linearly. The r's obtained by geometric spacing are represented by

$$r_n = r_{min}\left[\left(\frac{r_{max}}{r_{min}}\right)^{1/m}\right]^{n-1} \qquad (6)$$

or alternatively for linear spacing

$$r_n = r_{min} + (n-1)\left[\frac{r_{max} - r_{min}}{m}\right] \qquad (7)$$

where m is the total number of radii. Thus the program minimizes "var" given by

$$\text{var} = [I(Q) - \sum_{n=1}^{m} a_n I(Q,r_n)_{TH}]^2 \qquad (8)$$

where a_n is constrained to be positive and represents the amplitudes of a histogram.

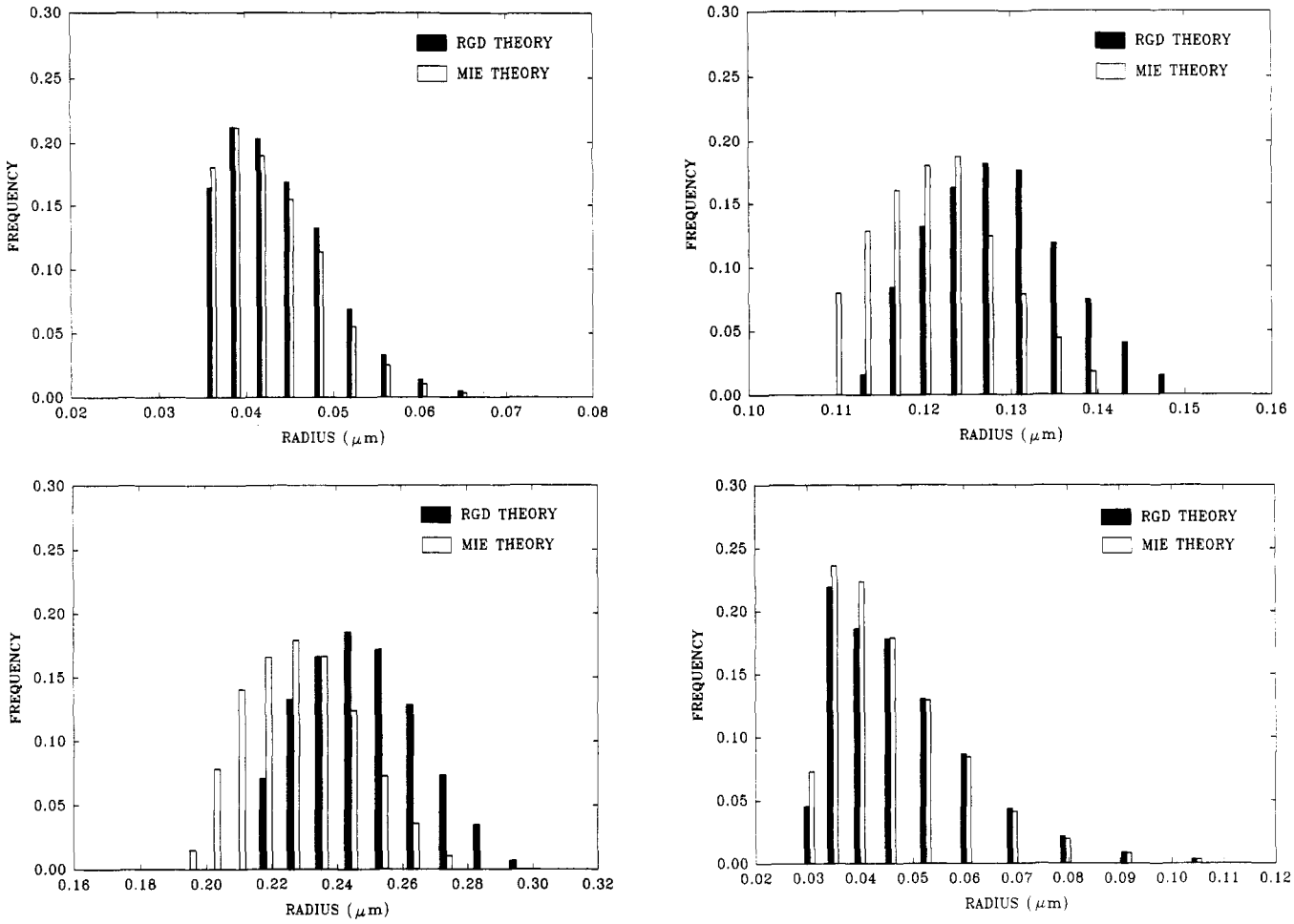

Figure 2. Histograms showing the size number distributions obtained from the fits represented in Figure 1 where A–D are described in Figure 1. As expected, the RGD approximation is valid for smaller particles but begins to overestimate the size for larger particles. Note that the histograms are not normalized to each other.

Experimental Design

The fiber optic based ILS spectrometer described elsewhere in detail[26] was used to generate $I(Q)$ vs Q data on several solid and hollow sphere systems. Two recent refinements to the existing spectrometer have greatly improved the signal sensitivity: a right-angled prism used to deflect the beam after it has passed through the sample cuvette reduces the unwanted flare which can make up a substantial percentage of the signal at smaller scattering angles and an analog-to-digital card placed in the control computer to monitor incident beam fluctuations. The light source was a continuous-wave, tunable argon ion Lexel (Model 95) laser set to a wavelength of 488 nm. The temperature reservoir was maintained at 29 °C for all experiments, except those involving vesicles, which were performed at 26 °C. The data collection time for each experiment was ~20 min. This represented the average of five short experiments consisting of complete passes of all 20 fixed scattering angles. This provides confidence in reproducibility and the ability to discard a particular run if, for example, a piece of dust should enter the scattering volume or a disturbance in the line voltage temporarily affects the electronics.

The 0.096- and 0.269-μm-diameter latex sphere standards were obtained from Duke Scientific Corp. (Palo Alto, CA). The 0.096-μm spheres (lot no. 9918) had a certified diameter of 0.096 μm with an uncertainty of 0.0039 μm determined by photon correlation spectroscopy, and the 0.269-μm spheres (lot no. 12240) had a certified diameter of 0.269 μm with an uncertainty of 0.007 μm as determined by transmission electron microscopy (TEM) by the National Institute of Standards and Technology (NIST). The hollow latex sphere samples were obtained from A. Rudin (Chemistry Department, University of Waterloo, Waterloo, Ontario, Canada). The suspensions were sonicated for 30 s and then diluted to the appropriate concentration for the light scattering experiments. The refractive indices for the hollow latex spheres are given for the lumen or inside the hollow sphere as $n_1 = 1.33$ (water), for the coat as $n_2 = 1.59$ (polystyrene), and for the medium (also water) as $n_0 = 1.33$). The shell thickness was approximated as 0.1 μm based on previous TEM studies[11] which also indicated that the shell thickness was reasonably constant regardless of sphere diameter.

The phospholipid vesicle preparations were performed in our own laboratory by the method of extrusion. The design of the extruder was based on a description of an extruder by Lipex Biomembranes Inc. (Vancouver, BC, Canada). In brief, 1,2-dipalmitoyl-*sn*-3-glycerophosphatidylcholine (DPPC) obtained from Avanti Polar Lipids, Inc. (Alabaster, AL), was mixed with cholesterol using dichloromethane and then placed in a rotary evaporator (Brinkmann Rotavapor R-110). The cholesterol increases the mechanical stability of the vesicles and allows the experiment to be run at temperatures much lower than is possible for pure DPPC vesicles. The appropriate amount of lipid is weighed and added to 5 mL of 750 mM NaCl to achieve a concentration of 5 mg/mL. The contents are then incubated in an oven at 48 °C for ~30 min prior to extrusion. The extruder has two temperature-controlled jackets, set to 48 °C, which are placed around the extruder itself and the collection test tube. The extruder is flushed through several times with 750 mM NaCl, and then ~2 mL of the dispersion is placed in the extruder and extruded at 200 psi through a single[27] 0.1-μm Nuclepore filter obtained from Costar (Cambridge, MA) a total of ten times.[28] This produces a stock solution of DPPC/cholesterol vesicles, which is then diluted to the appropriate experimental concentration while maintaining an isotonic solution. The refractive index of the lipid was 1.431, and the refractive index of the 750 mM NaCl solution was 1.341. The thickness of the lipid bilayer was assumed to be 0.007 μm, assuming the vesicles to be unilamellar, which has been confirmed by nuclear magnetic resonance (NMR) spectroscopy. The relative loss of ^{31}P signal in the presence of Mn^{2+} provides a measure of the average number

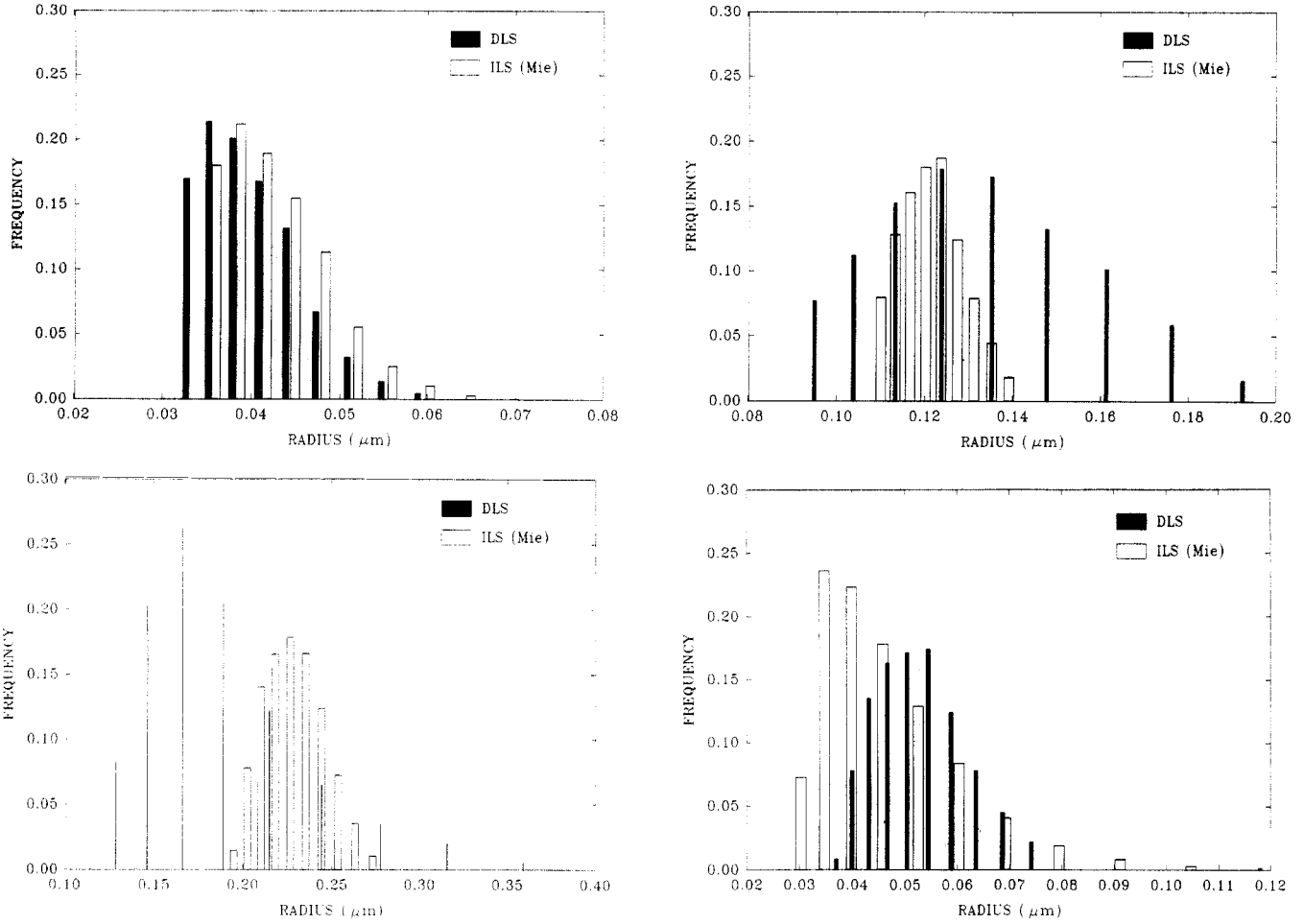

Figure 3. Histograms showing the size number distributions for both ILS (using Mie theory) and DLS where A–D are described in Figure 1.

Table 2. Mean and Standard Deviations Obtained from the Histograms for both the Solid and Hollow Spheres for 0, 1, 2, and 5% Random error

	0% random error		1% random error		2% random error		5% random error	
sample	r_2 (μm)	std dev (μm)	r_2 (μm)	std dev (μm)	r_2 (μm)	std dev (μm)	r_2 (μm)	std dev (μm)
solid sphere	0.051	0.0072	0.051	0.0073	0.050	0.0073	0.051	0.0070
hollow sphere	0.050	0.0077	0.050	0.0081	0.050	0.0087	0.050	0.0105

of lipid bilayers per vesicle.[29] The results indicated that ~95% of the 0.1-μm vesicles made by our extrusion technique were unilamellar.

Dynamic light scattering (DLS) experiments were performed using an apparatus and methods which have been described in detail elsewhere.[9] All data analysis was performed on a microcomputer using the FORTRAN programming language. The analysis incorporates the scattering factors for coated spheres[10] as well as mass corrections. The final distributions that were obtained were number distributions in the form of histograms.

The ILS size distribution program, also written in FORTRAN, calculates number distributions for both solid and hollow spheres using either the RGD or Mie theories. The user inputs a size range over which the fit will take place and the program divides up the size domain either linearly or geometrically into a maximum of 75 discrete radii. The program was found to be more robutst by dividing the size domain into five passes of up to 15 discrete radii and then renormalizing each pass. The geometric spacing increases the proportion of smaller to larger radii, which enhances the sensitivity to smaller particles present since they produce a less significant effect on the intensity function than do larger spheres (especially for bimodal distributions). Linear spacing was investigated but the quality of the fit was superior using geometric spacing. Depending on the quality of the data, the number of discrete radii chosen becomes important. If the size domain is divided into too many radii, the program will begin to fit the noise in the data, contributing to unreliable results. If the size domain is not divided into enough discrete radii, the resultant distribution can be uncharacteristically wide and could, for example, leave two size distributions close together, unresolved. The initial r_{min} should be chosen sufficiently small (~0.01 μm) to investigate for smaller particles, and r_{max} should be chosen sufficiently large (~2 μm) to monitor larger particles. The program outputs a number distribution in the form of a histogram, the fitted form of $I(Q)$, and information on the moments of the distribution. This information is used to determine the confidence and quality of the fit. The best fit will be obtained by choosing values for r_{min} and r_{max} which produce the smallest sum of squares, while not fitting to the experimental noise.

Experimental Results and Discussion

The experimental $I(Q)$ vs Q data plotted with the RGD and Mie results produced by the fitting program are shown in Figure 1. The 0.096-μm solid spheres, 0.269-μm solid spheres, hollow latex spheres, and vesicle data are represented by A–D, respectively. The fits obtained using both theories are in good agreement with the experimental results, except for the larger hollow spheres where the RGD approximation is no longer valid. The histograms representing the number distributions obtained by the fit comparing the RGD and Mie theories are shown in Figure 2A–D. As expected, the RGD theory performs well for

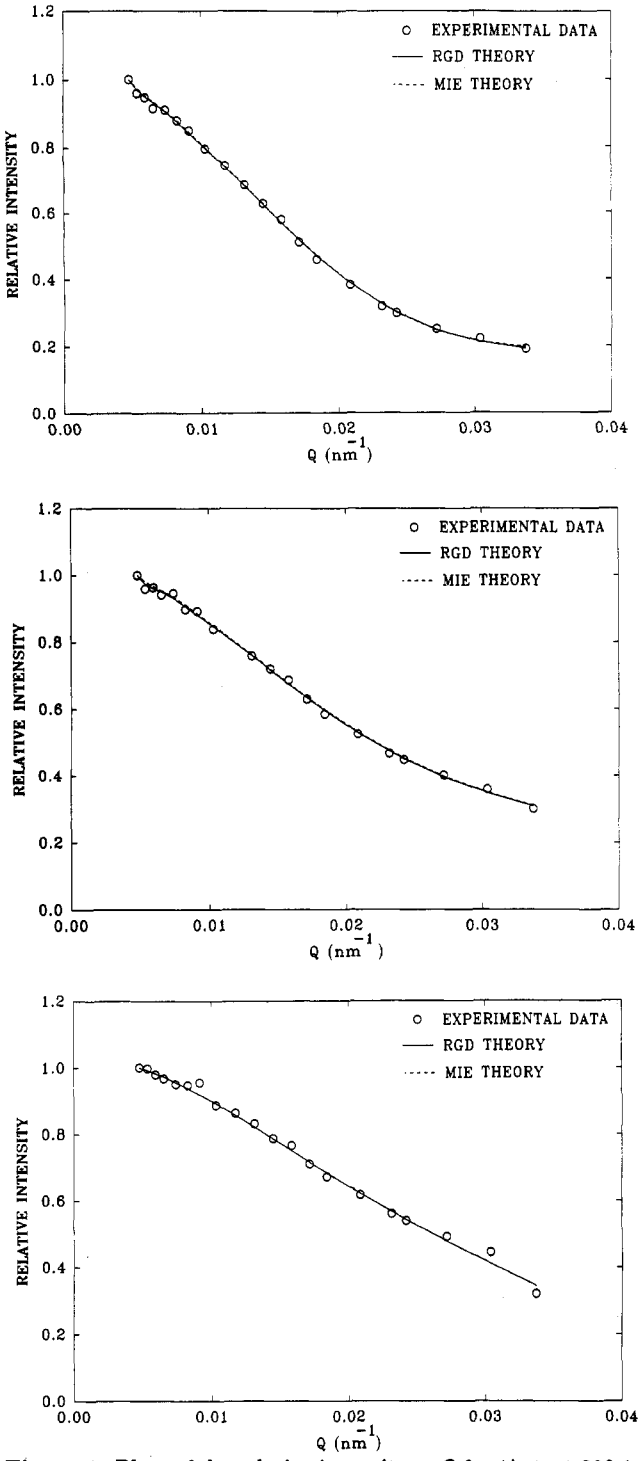

Figure 4. Plots of the relative intensity vs Q for (A, top) 200:1, (B, middle) 500:1, and (C, bottom) 800:1 mixtures of 0.096- and 0.269-μm solid latex spheres comparing both the RGD and Mie theories.

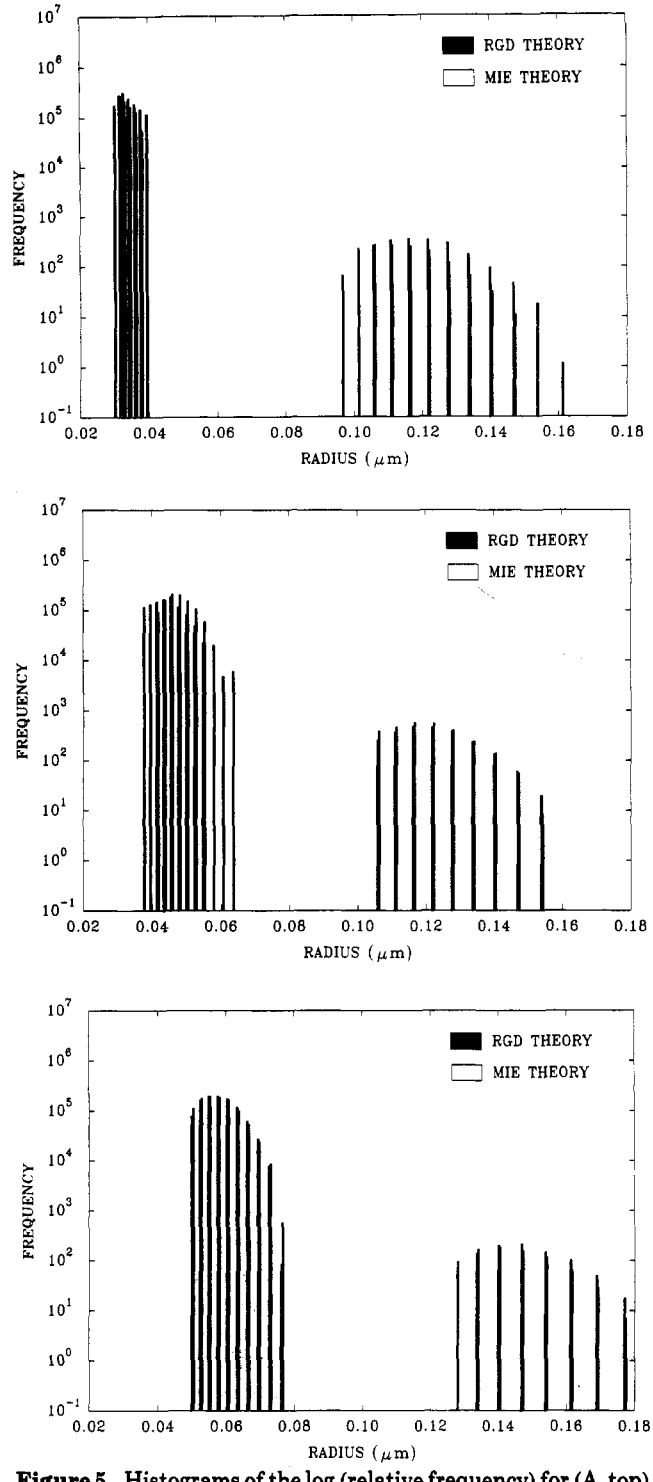

Figure 5. Histograms of the log (relative frequency) for (A, top) 200:1, (B, middle) 500:1, and (C, bottom) 800:1 mixtures obtained by the fits shown in Figure 4 to enhance the bimodal distribution.

the smaller particles but begins to overestimate particle size for larger particles (see Table 1).

In Figure 3A–D a comparison between the Mie and DLS results shows that in every case except that of vesicles the width of the distribution is reduced, suggesting that ILS spectroscopy may offer greater resolution. Three possible explanations may account for the differences in distribution width. First of all, by increasing the DLS data collection time, the resolution may be enhanced. However, the DLS data shown here were already the result of ~12 h of data collection. It would seem impractical to collect data for longer periods of time, especially for dynamic systems like vesicles where their stability would be in question for run times this long. The other explanations arise from characteristics of the technique, namely, the data collection process and the size distribution analysis. First, for the ILS apparatus the experimental noise at each angle is independent. However, this is not true for the autocorrelation function obtained by DLS (where statistical errors are correlated). Second, the data analysis for the ILS technique fits to Bessel functions, which may be less difficult than fitting exponentials. As already stated, the vesicle data would appear to be the exception. This may be explained by recent electron micrographs which have shown that in isotonic preparations some vesicles are ellipsoidal until osmotic pressure which induces swelling gives the vesicles a spherical shape.[30] The ILS technique may be more sensitive to shape variations which produce quite different scattering characteristics, whereas

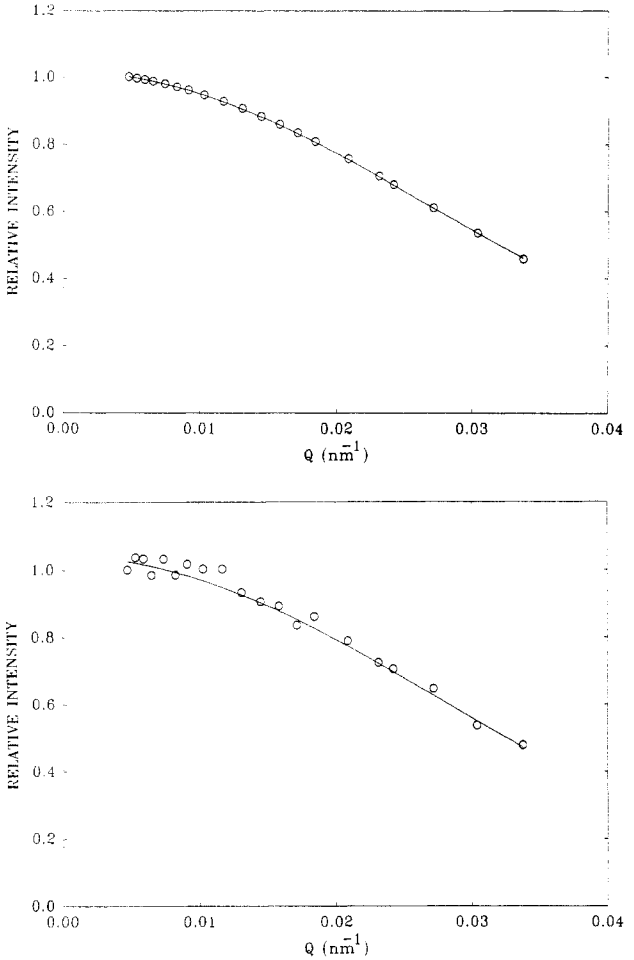

Figure 6. Plots of the relative intensity vs Q for (A, top) 0% and (B, bottom) 5% random error showing the fit obtained by the size distribution program using the Mie theory for solid spheres of mean radius 0.048 μm.

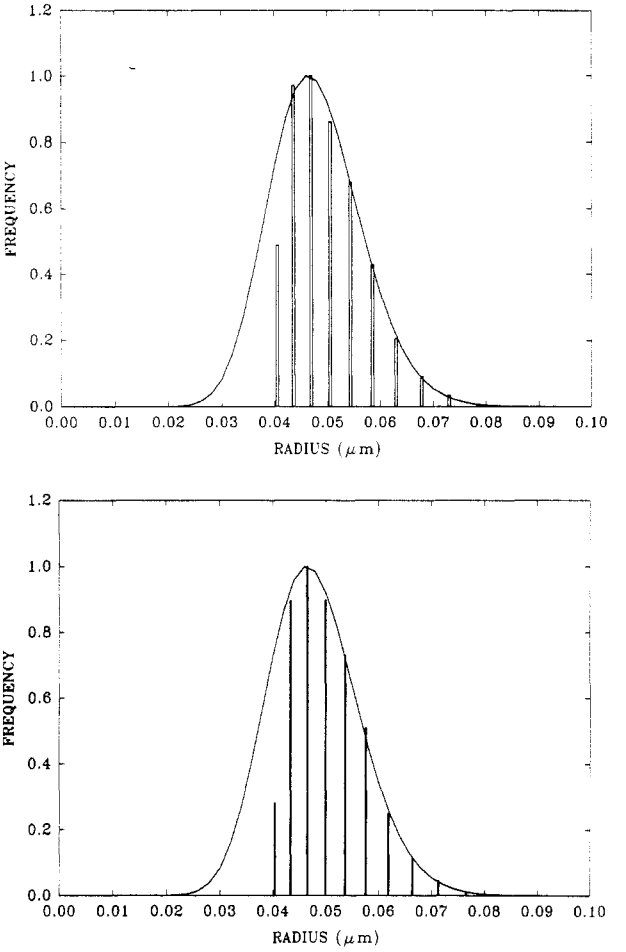

Figure 7. Histograms showing the size number distributions obtained from the fits represented in Figure 6.

the rotationally averaged diffusive motions measured by DLS would be essentially unaffected for particles of this size.

Results pertaining to three different mixtures of 0.096- and 0.269-μm solid latex spheres are shown in Figures 4 and 5. To accurately determine the sizes of a bimodal sample, the particle populations were adjusted such that the scattering intensity was approximately the same for both sizes. Since the scattering intensity increases roughly as r^6, this would represent a mixture of 500:1 (i.e., ~500 0.096-μm spheres for every 0.269-μm sphere). Shown here are the results of three different mixture ratios of approximately 200:1, 500:1, and 800:1. In each case bimodal distributions are produced, but the 500:1 mixing ratio is in better agreement with results obtained from the unimodal distributions shown earlier. For the 200:1 mixture the larger particles are easily distinguished, but ILS underestimates the size of the smaller particles. For the 800:1 mixture it overestimates both particle sizes. For DLS it is also important to choose appropriate mixing ratios to obtain accurate results. The DLS technique can be prone to error because of difficulties in bin time optimization and potential number fluctuations in the largest particle sizes.

Since the experimental data include noise, the sensitivity of the inversion technique was tested on a solid sphere and hollow sphere polydisperse distribution containing different percentages of random noise. A distribution function which in previous studies[31] was found to characterize typical distributions of particles in the 0.05–0.1-μm radius range is given by

$$G(r) = \frac{r^m}{m!}\exp\left[-r\left(\frac{m+1}{R}\right)\right] \quad (9)$$

where R is the mean radius of the distribution and m controls the width. The distribution shown in Figures 7 and 9 was generated using $m = 30$ and $R = 0.048$ μm over a range of $r = 0$–0.1 μm. Particle radii starting from 0.026 to 0.076 μm in increments of 0.002 were input into the Mie scattering function (eq 3) for both a solid sphere and a hollow sphere model. Refractive indices of $n_0 = 1.33$ and $n_1 = n_2 = 1.59$ (latex) were used to describe the solid sphere, and $n_0 = n_1 = 1.33$ and a coat refractive index $n_2 = 1.45$ were used for the hollow sphere case with a coat thickness of 0.007 μm. The values obtained by the Mie theory for the scattering angles measured by the ILS spectrometer were then multiplied by the appropriate coefficients representative of the generated distribution and added together to obtain polydisperse $I(Q)$ vs Q plots (see Figures 6A and 8A).

The data files representative of the $I(Q)$ vs Q plots were then used to produce simulated data files containing 0, 1, 2, and 5% random error for both the solid and hollow spheres. These data files were then input into the ILS size distribution program. The resultant $I(Q)$ vs Q best fit functions and the input functions are compared in Figure 6 for the solid spheres and Figure 8 for the hollow spheres where (A) and (B) represent 0% and 5% added noise, respectively. The corresponding histograms are shown in Figure 7 for the solid spheres and Figure 9 for the hollow spheres. It appears that, by introducing random errors of even up to 5%, the inversion technique is robust enough to yield accurate size distributions for both the

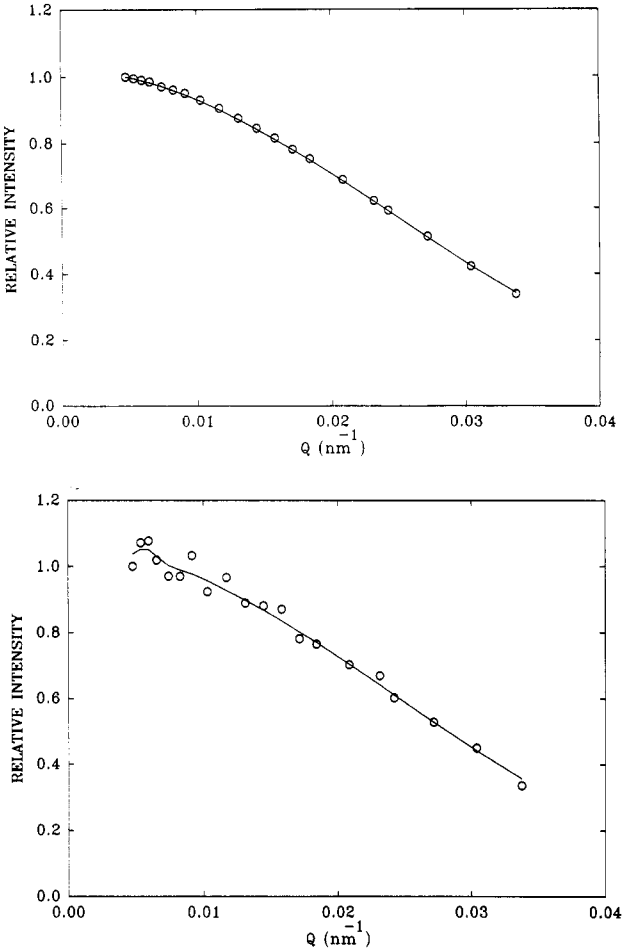

Figure 8. Plots of the relative intensity vs. Q for (A, top) 0% and (B, bottom) 5% random error showing the fit obtained by the size distribution program using the Mie theory for hollow spheres of mean radius 0.048 μm.

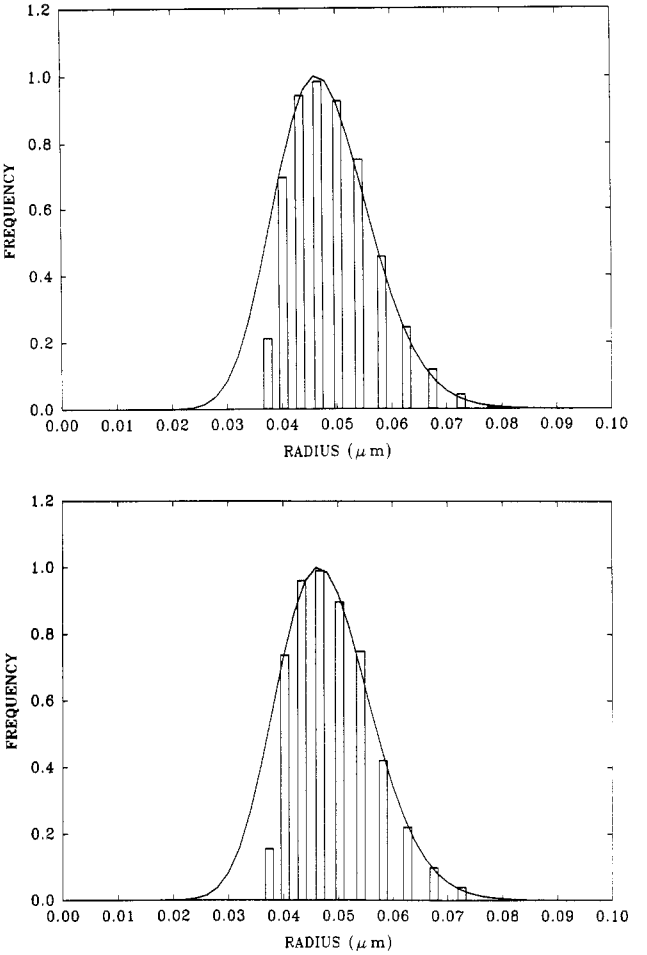

Figure 9. Histograms showing the size number distributions obtained from the fits represented in Figure 8.

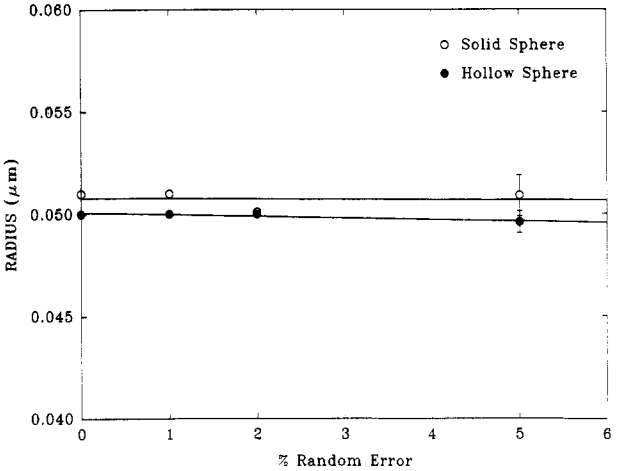

Figure 10. Plot of mean radius vs percent random error for (○) solid spheres and (●) hollow spheres. The values were obtained from Table 2.

solid and hollow spheres (see also Table 2).

In Figure 10 the mean radius is plotted as a function of percent random error. The solid and hollow spheres show little effect from the inclusion of random noise. The differences obtained in the mean radius and standard deviation due to random error still represent only a few nanometers. Error bars displayed on the 5% random error points should scale down for the smaller percentages of random error. The mean value and size of the error bars were determined by evaluating ten independent scattering functions created with 5% random error.

The overall performance and robustness of the program give a great deal of confidence to the size distribution information obtained. It is always important to observe the $I(Q)$ vs Q plot and its respective fit when interpreting the information given by the histogram. With random errors of even up to 5%, which would represent very poor quality data, it appears that the inversion technique performs favorably.

Conclusion

ILS spectroscopy offers many advantages over DLS spectroscopy for the determination of particle size distributions, even though the accuracy of DLS spectroscopy as a particle-sizing technique has been well accepted and documented in recent years. In particular, number distributions are obtained directly, with enhanced resolution, while significantly reducing experimental run time. This is a direct result of the experimental noise being independent for each scattering angle. Although the RGD theory provided adequate results, for smaller particles, the Mie theory is more accurate and reliable, and with the computing power available today, the Mie theory can be applied without a substantial increase in fit time. However, DLS experiments depend only on particle diffusion and do not require any instrumental calibration. While ILS may be faster and more sensitive, the quality and accuracy of the recovered distributions depend on the accuracy of the calibration.

Acknowledgment. We acknowledge the participation in this effort of J. Marsh, who performed all the DLS analysis. This project was supported by a grant from the

Natural Sciences and Engineering Research Council of Canada.

References and Notes

(1) Selser, J. C.; Yeh, Y. *Biophys. J.* **1976**, *16*, 847.
(2) Goll, J. H.; Stock, G. B. *Biophys. J.* **1977**, *19*, 265.
(3) Goll, J. H.; Carlson, F. D.; Barenholz, Y.; Litman, B. J.; Thompson, T. E. *Biophys. J.* **1982**, *38*, 7.
(4) Ruf, H.; Georgalis, Y.; Grell, E. *Methods Enzymol.* **1989**, *172*, 362.
(5) McCracken, M. S.; Sammons, M. C. *J. Pharm. Sci.* **1987**, *76*, 56.
(6) Rouch, J.; Safouane, A.; Tartaglia, P.; Chen, S.-H. *J. Chem. Phys.* **1989**, *90*, (7),. 3756.
(7) Burchard, W. *Makromol. Chem., Macromol. Symp.* **1988**, *18*, 1.
(8) Helmstedt, M. *Makromol. Chem., Macromol. Symp.* **1988**, *18*, 37.
(9) Hallett, F. R.; Craig, T.; Marsh, J.; Nickel, B. G. *Can. J. Spectrosc.* **1989**, *34*, 63.
(10) Hallett, F. R.; Watton, J.; Krygsman, P. *Biophys. J.* **1991**, *59*, 357.
(11) Strawbridge, K. B.; Hallett, F. R. *Can. J. Phys.* **1992**, *70*, 401.
(12) Sheu, E. Y. *Phys. Rev. A* **1992**, *45* (4), 2428.
(13) Finsy, R.; Deriemaeker, L.; Gelade, E.; Joosten, J. *J. Colloid Interface Sci.* **1992**, *153* (2), 337.
(14) Schnablegger, H.; Glatter, O. *J. Colloid Interface Sci.* **1993**, *158*, 228.
(15) Pike, E. R.; Watson, D.; Watson, F. M. *Measurement of Suspended Particles by Quasi-Elastic Light Scattering*; Dahneke, B. E., Ed.; John Wiley and Sons: New York, 1983.
(16) Morrison, I. D.; Grabowski, E. F.; Herb, C. A. *Langmuir* **1985**, *1*, 496.
(17) Lord Rayleigh, *Philos. Mag.* **1981**, *12*, 81.
(18) Lord Rayleigh, *Proc. R. Soc. London* **1910**, *A84*, 25.
(19) Lord Rayleigh, *Proc. R. Soc. London* **1914**, *A90*, 219.
(20) Lord Rayleigh, *Proc. Roy. Soc. London* **1918**, *A94*, 296.
(21) Debye, P. *Ann. Phys.* **1915**, *46*, 809.
(22) Gans, R. *Ann. Phys.* **1925**, *76*, 29.
(23) Wyatt, P. J. In *Methods of Microbiology*; Norris, J. R., Ribbons, D. W., Eds.; Academic Press: New York, 1973.
(24) Mie, G. *Ann. Phys.* **1908**, *25*, 377.
(25) Bohren, C. F.; Huffman, D. R. *Absorption and Scattering of Light by Small Particles*; John Wiley and Sons: New York, 1983.
(26) Strawbridge, K. B.; Hallett, F. R.; Watton, J. *Can. J. Spectrosc.* **1991**, *36* (3), 53.
(27) Chapman, C. J.; Erdahl, W. L.; Taylor, R. W.; Pfeiffer, D. R. *Chem. Phys. Lipids* **1990**, *55*, 73.
(28) Mayer, L. D.; Hope, M. J.; Cullis, P. R. *Biochim. Biophys. Acta* **1986**, *858*, 161.
(29) Bergelson, L. D.; Barsukov, L. I. *Science (Washington, D.C.)* **1977**, *197*, 224.
(30) Mui, B. L.-S.; Cullis, P. R.; Evans, E. A.; Madden, T. D. *Biophys. J.* **1993**, *64*, 443.
(31) Hallett, F. R.; Marsh, J.; Nickel, B. G.; Wood, J. M. *Biophys. J.* **1993**, *64*, 435.